Available online at www.eccomasproceedia.org
Eccomas Proceedia COMPDYN (2021) 4058-4077

ECCOMAS
Proceedia

COMPDYN 2021
8th ECCOMAS Thematic Conference on
Computational Methods in Structural Dynamics and Earthquake Engineering
M. Papadrakakis, M. Fragiadakis (eds.)
Streamed from Athens, Greece, 28 - 30 June 2021

SEISMIC RETROFIT OF EXISTING PRECAST RC BUILDINGS WITH DISSIPATIVE DEVICES BASED ON CARBON WRAPPED STEEL TUBES

Lucia Praticò[1], Andrea Vittorio Pollini[2], Devis Sonda[2] and Nicola Buratti[1]

[1] University of Bologna, DICAM Department
Viale Risorgimento 2, 40136 Bologna - Italy
{lucia.pratico3, nicola.buratti}@unibo.it

[2] Sismo Solution s.r.l.
Viale Carlo Pepoli 82, 40123 Bologna - Italy
{apollini, dsonda}@sismosolution.com

Abstract

The seismic vulnerability of existing precast RC buildings not designed against seismic actions is a well-known issue nowadays, as emerged from the aftermath of the seismic events that affected many productive areas in the Emilia region (north Italy) in 2012. This is a consequence of the lack of structural redundancy and the widespread adoption of friction-based connections, which can lead to collapses and significant damage to contents. Thus, the necessity of identifying suitable intervention strategies has been widely recognized by researchers, which proposed different retrofit techniques. One of the most diffused approaches is to introduce mechanical connectors between columns and roof elements, resulting in an increase of the base shear and the need to strengthen the columns. To prevent this phenomenon, dissipative devices based on Carbon-Wrapped Steel Tubes (CWST) are introduced herein for the retrofit of existing precast RC structures, aiming at reducing the forces transmitted to columns, and providing a suitable connection between columns and beams. To this regard, this paper discusses the seismic retrofit of an existing precast building equipped with CWSTs. Linear and non-linear time history analyses have been conducted on two different models of the structure, one with hinged beam-column connections, and on the one with CWSTs. The yielding and the ultimate rotations of the plastic hinges at the base of the columns as well as the cyclic shear resistance depending on the ductility demand on each element, are defined according to Eurocode 8 prescriptions. The paper discusses the effects of the introduction of the CWSTs in the connections in terms of forces and proposes equivalent behavior factor values for the two structures.

Keywords: Precast RC buildings, Dissipative devices, Seismic retrofitting, NLTH analysis, Behavior factor

ISSN:2623-3347
Peer-review under responsibility of the organizing committee of COMPDYN 2021.
doi: 10.7712/120121.8767.19292

1 INTRODUCTION

Since the 1970s, precast Reinforced Concrete (RC) structures have been widely used in many countries for one-story industrial buildings such as warehouses and factories. The seismic vulnerability of existing precast RC buildings built without seismic-design criteria is a well-known issue nowadays, as highlighted by damage occurred after the 2012 Northern Italy earthquakes that affected many productive areas [1, 2, 3, 4, 5]. The main source of vulnerability of these structures is the lack of effective mechanical connectors between their structural elements, indeed friction-based connections were widespread [6, 7, 8, 9, 10]. Friction-based connections are not able to guarantee an effective shear force transmission, causing loss of support failures and collapses; moreover, the simultaneous effect of the horizontal and vertical components of the seismic action can increase the probability of occurrence of this type of failure [11]. The vulnerability of structures characterized by these frictional connections has been confirmed by numerous numerical simulations [8, 10, 12, 13, 14, 15]. In addition, the failure of beam-column connections based on friction only, can frequently occur before the development of plastic hinges at the base of columns, causing undesired non-ductile failure modes, as reported in Deyanova et al. [16].

Given the high vulnerability of friction-based connections and the economic significance of prefabricated RC structures, many strengthening solutions have been proposed in the literature [6, 8, 17, 18, 19]. The reduction of damage and collapses due to seismic events for this type of structures, becomes even more strategical since a high economic impact due to industrial business interruption has to be taken in account, in addition to the direct economic losses [20, 21, 22]. All the strengthening solutions are typically based on the introduction of steel ties, plates, or cable restraints, to avoid sliding of the beams and therefore unseating failures. Most of these solutions aim only at converting friction-based connections into hinged connections with no focus on energy dissipation, and therefore they often require the strengthening of the base of columns.

Thus, *ad hoc* solutions based on different energy dissipation mechanisms have been proposed. For instance, Dal Lago et al. [23, 24, 25] proposed to concentrate energy dissipation in simple and rather inexpensive elements, such as steel angles connectors. Scotta et al. [26] focused on the dissipative role of cladding panels acting as shear walls; Belleri et al. [27] introduced energy dissipation in hinged connection, suggesting a re-centering dissipative devices based on rotary friction; Martinelli and Mulas [28] proposed a similar solution involving the insertion of devices dissipating energy through rotary friction, with no re-centering capacity. Alternative solutions are based on the introduction of dampers, as suggested by Marinini et al. [29].

In this context, the present paper refers to a low-damage solution for the retrofit of beam-column connections of existing precast RC structures, proposing the introduction of dissipative fuse devices based on Carbon-Wrapped Steel Tubes (CWST), introduced in Pollini et al. [30, 31]. Pollini et al. [32] presented an analytical simplified approach to estimate an equivalent behavior factor to be used in design applications with these devices, validated by comparison with a large number of incremental dynamic analyses (IDAs).

In this paper, the evaluation of the improvement in the seismic behavior of an existing precast RC building retrofitted with CWST devices is proposed, through comparative considerations on the behavior factor calculated for the existing structure, and for the one after the intervention. The first part of the paper presents the properties of the dissipative fuse devices adopted for the retrofit intervention of the main frame of the building. Thus, the modelling strategies are described in detail, as well as the development of the non-linear time history analyses. Finally, the results in terms of behavior factor quantification, for the current structure and

for the retrofitted one, are proposed and discussed with the aim of evaluating the effects of the CWSTs in the reduction of the seismic vulnerability of the building.

2 CWST DISSIPATIVE DEVICES

The dissipative fuse devices based on CWSTs [31, 32] considered in the present paper have two main purposes: (i) to connect beam-column joints in order to prevent the possible unseating failure of beams, and (ii) to act as dissipative fuses, thus reducing the effects of seismic actions on structural elements. Specific studies in automotive engineering on structural crashworthiness [33, 34] showed that metals, combined with composite materials in thin-walled circular tubes, have excellent capacities of energy absorption under axial compressive loads. From these, the CWST devices were developed, and an example of a real application can be seen in Figure 1a.

(a) (b)

Figure 1: (a) Example of a beam-column connection provided with coupled CWST dissipative devices; (b) single fuse device made of carbon-wrapped steel tubes.

It is worth noticing that, since each CWST (Figure 1b) dissipates energy only under compressive loading, two devices must be positioned at each beam-column joint. A threaded bar is placed through the CWSTs in order to guide their displacement, and also to ease their connection to structural elements. In this way, standard steel anchoring elements can be used to fix the threaded bar to the column. Moreover, the anchorage on the beam is guaranteed by a significantly stiff and strong steel element, able to transfer forces from beams to the CWSTs.

The CWST device works firstly in the elastic range, like a fuse restraint avoiding relative displacement between two structural components, below a certain pre-established force threshold. Above this threshold, the plastic deformation of the device begins (plasticization phase), as well as the energy dissipation.

In order to understand the behavior of the devices, in Figure 2a the force-deformation diagram of a single CWST in compression is proposed [31]. In the Figure, F_{eq} is the equivalent plastic force threshold, and S_{max} is the maximum deformation capacity. The behavior of a connection with a CWST device can be described within three main steps. In the initial branch O-A the device remains elastic, and the lateral seismic force is fully taken by the column. As soon as the force overcome F_{eq} (branch A-B of the curve), the device starts to buckle and the plastic deformation develops, while a constant value of the force is transmitted to the column. After point B, when the device attains its maximum deformation capacity, the stiffness boosts significantly. At this step, the device performs as a displacement-limiter between beams and columns,

thanks to the aforementioned threaded bar, thus, from this point, the columns fully bears the seismic load and start to deform and yield (typically at the base).

In case of ground motions, and in general under cyclic loading, the two CWSTs positioned in one joint, work alternatively. Figure 2b represents the force-deformation law of a couple of devices in case of cyclic loads. In the picture, the red path shows that, when a load reversal occurs after entering the plastic branch of one of the devices, the connection slides with no force until the recovery of the entire deformation.

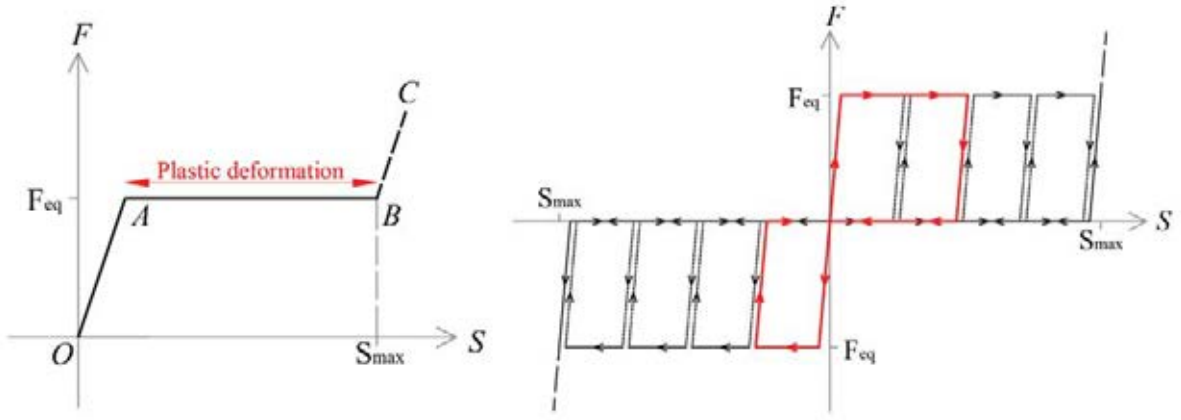

(a) (b)

Figure 2: Force-deformation behavior of the CWST device: (a) single device behavior under compression; (b) hysteretic behavior of two devices under cyclic loading.

3 FEM MODELS OF THE PRECAST RC FRAME

The seismic retrofit with CWST devices is herein applied to an existing precast RC building located in Carpi (MO), in the Emilia Romagna region (Italy). The building was built in the ’70, and features double span main frames constituted by I-shaped precast beams, simply supported on rectangular precast columns. After the seismic events of May 2012, the building was subjected to a temporary retrofit solution with steel plates applied at the beam-column joints, aimed to prevent the unseating of the precast elements. It is worth noticing that the retrofit with CWSTs discussed in this work, has the purpose of improving the seismic behavior of the building with respect to the current condition.

The roof slab is made by simply supported hollow-clay elements, without a rigid concrete slab, thus, the structural scheme lacks structural redundancy, consisting in simply supported beams and cantilever columns [35, 36]. Since the building is simple and regular in plan, and there is not a rigid diaphragm at the roof level, the seismic behavior of the entire building can be approximated with the 2D model of one of the internal main frames, in the direction of the beams. In the orthogonal direction, a different retrofit solution was adopted.

In order to evaluate the effects of the retrofit intervention, two different frames are modelled with finite elements, with the software Midas GEN [37]:

A) main frame of the building with hinged beam-column connections, representing the structure in the current condition with the temporary retrofit solution (Figure 3a);

B) main frame of the building with CWST devices placed at the beam-column joints, representing the retrofitted structure (Figure 3b). In this last model, appropriate *link* elements, i.e. nonlinear springs, are used in order to model the behavior of the dissipative devices, as explained in the following sections.

The frames are subjected to seven horizontal recorded ground-motion accelerograms, according to Eurocodes prescriptions for safety verifications of existing buildings with non-linear analyses [38, 39], as furtherly described in Section 4.1. The vertical seismic action is not considered in this work.

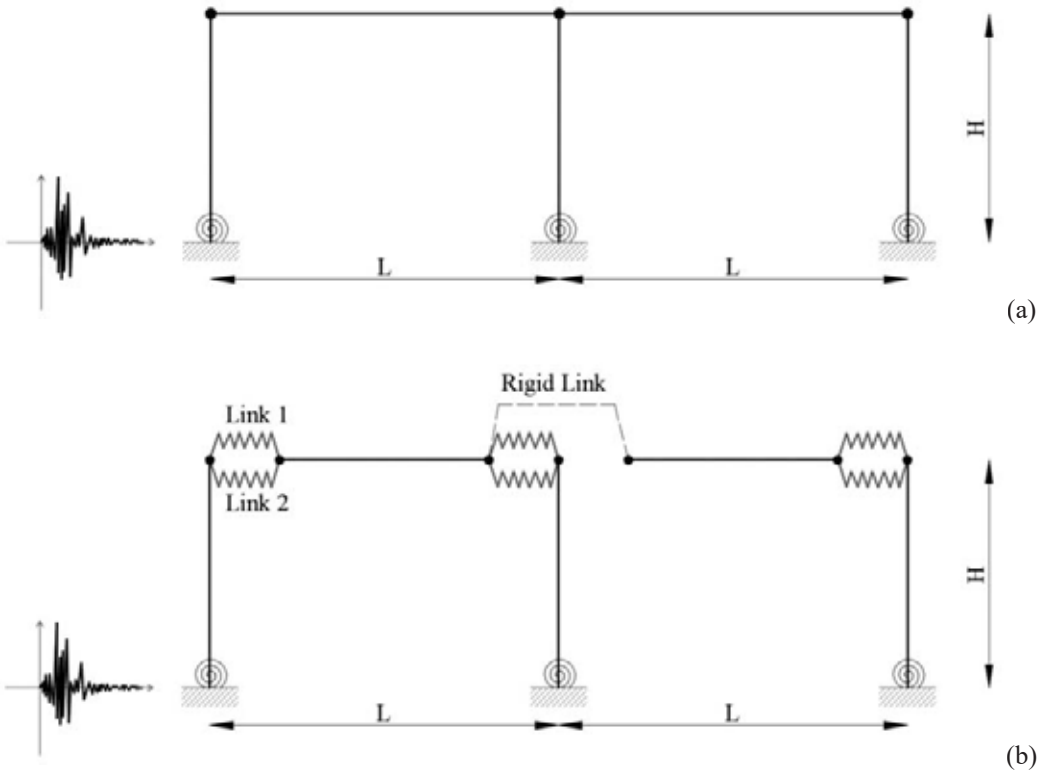

Figure 3: Structural FEM models adopted in the analyses: a) model A representing the existing structure; b) model B representing the frame retrofitted with CWSTs.

The main frame illustrated features two spans of 21.8 m, with precast main beams characterized by sections with depth spanning from 0.8 m at their ends to 1.6 m at mid-span. The three columns are 5.5 m high, with a rectangular section of 40 x 54 cm. Mechanical steel connectors are present between beams and columns, allowing to consider a rigid hinged connection between the elements in the existing condition.

The gravity loads are computed in the seismic combination of actions [38] according to the influence area of each element, and transformed into lumped masses for the dynamic analyses. The axial load ratio, computed in the seismic combination of loads, is 0.033 for the two external columns, and 0.063 for the internal. The material properties have been estimated according to in-situ testing reports, showing a concrete class C32/40 and a steel class FeB44k for the column reinforcement.

Since the building was built before the introduction of seismic design criteria in the region, the columns exhibit low seismic detailing and in particular poor transverse reinforcement. Indeed, the columns are reinforced with 4Φ14 ribbed bars with 2.5 cm concrete cover, and 2 additional Φ6 located along the height of the section, confined with transversal stirrups Φ6 spaced 20 cm. The columns are modelled clamped at their base, since, due to the presence of a rigid industrial floor, the interaction with the foundation is not under analysis in this work. At the base of columns, non-linear lumped plastic hinges are modelled adopting trilinear moment-rotation relationships, defined according to Eurocode 8 formulations for reinforced concrete structures [39]. The shear resistance of the columns is computed following the expression for

cyclic shear resistance calculation in Eurocode 8 [39], depending on the ductility demand of each element. It is worth noticing that, in all models, beams have a linear behavior since no damage is expected to occur in these elements.

3.1 Properties of the plastic hinges

The non-linear flexural behavior of columns is taken into account by means of plastic hinges at their base. Trilinear moment-rotation rules are implemented, considering the cracking point (θ_{cr}, M_{cr}), the yielding point (θ_y, M_y), and the ultimate point (θ_u, M_u), with a perfectly plastic post-yielding behavior. The hysteresis model considered is a symmetric Takeda rule [40] able to represent the stiffness degradation of the elements, with an exponent in unloading stiffness equal to 0.4, and an inner loop unloading stiffness reduction factor equal to 1.

The value of the chord rotation at cracking is calculated as the ratio between the cracking moment and the elastic stiffness of a cantilever column with a fully reacting section. The yielding and the ultimate rotations at the life safety limit state are defined according to Biskinis and Fardis formulations [41, 42] adopted in Part 3 of Eurocode 8. The formulas are reported in Equations (1) and (2), respectively:

$$\theta_y = \phi_y \frac{L_V}{3} + 0.0013\left(1 + 1.5\frac{h}{L_V}\right) + 0.13\phi_y \frac{d_{bL} f_y}{\sqrt{f_c}} \tag{1}$$

$$\theta_{u,SLV} = \frac{3}{4}\frac{1}{\gamma_{el}} 0.016(0.3^{\nu}) \left[\frac{max(0.01;\omega')}{max(0.01;\omega)} f_c\right]^{0.225} \left(\frac{L_V}{h}\right)^{0.35} 25^{(\alpha\rho_{sx}\frac{f_{yw}}{f_c})} (1.25^{100\,\rho_d}) \tag{2}$$

where: ϕ_y is the yield curvature at the end section, L_V is the ratio moment/shear at the end section, h is the depth of the cross-section, d_{bL} is the mean diameter of the tension reinforcement, f_y and f_c are the steel yield stress and the concrete strength, respectively, γ_{el} is equal to 1.5 for primary seismic elements, ν is the axial load ratio, ω and ω' are the mechanical reinforcement ratios of the tension and compression, respectively, longitudinal reinforcements, α is the confinement effectiveness factor, ρ_{sx} is the ratio of transverse steel parallel to the direction of loading, f_{yw} is the stirrup yield strength, ρ_d is the steel ratio of diagonal reinforcement, if any, in each diagonal direction. It is worth noticing that the same materials and sections characterize the three columns, which differ only because of the axial load. Mean values of the material properties are adopted to calculate moments and rotations. Moreover, the shear span L_V is equal to the full column height. The coordinates of the characteristic points of the trilinear plastic hinges are reported in Table 1.

It is important to highlight that the expression used for the calculation of θ_u is defined for elements with ribbed bars and seismic detailing. The formula can be also adopted for elements that are not conforming to seismic codes, by applying reduction factors. In particular, empirical scaling factors are defined based on whether a member i) does not conform to modern seismic codes (22.9% reduction); ii) is not provided with properly anchored stirrups providing effective confinement (1.6% reduction); iii) has laps of longitudinal bars inside the plastic hinge region (from 15% to 66% reduction). This last factor significantly influences the calculation of the ultimate rotation [43], resulting in a reduction coefficient which increases if the lap is less than 40 diameters (in case of ribbed bars). For the case study frame, the first two empirical reduction coefficients are taken into account for the determination of θ_u. Since the columns are prefabricated, with continuous longitudinal bars, it is not possible to consider the third correcting coefficient. All this enhances the necessity to evaluate other types of significant reduction

coefficients to be proposed in this formula for the specific case of existing prefabricated elements not designed with anti-seismic standards, for which additional research may be required [44, 45].

In this work, in order to analyse the sensitivity of the results depending on the value of ultimate chord rotation considered, the authors consider the adoption of two alternative values corresponding to 80% and 60% of θ_u. Thus, the dynamic analyses are conducted with three different threshold values of rotations for both the models (i.e. model A and B), in order to evaluate the influence of this parameter on the estimation of the behavior factor. The values calculated for the case study frame are presented in Table 1.

	M_{cr} (kNm)	M_y (kNm)	M_u (kNm)	θ_{cr} (rad)	θ_y (rad)	θ_u (rad)	80% θ_u (rad)	60% θ_u (rad)
External column	70.5	236.6	236.6	0.00074	0.01412	0.03232	0.02586	0.01939
Internal column	70.5	297.5	297.5	0.00074	0.01462	0.03118	0.02495	0.01871

Table 1: Characteristic points of the moment-rotation relationships adopted for the external and the internal columns of the precast frame.

3.2 Shear resistance

The shear in columns is checked at each step of the analysis with respect to the shear resistance, as prescribed by Eurocode 8, avoiding the modelling of non-linear shear hinges. The formula adopted for the verification is given in Eurocode 8, part 3 [39]. It accounts for the cyclic shear resistance which decreases with the increase of the plastic ductility demand μ_Δ^{pl}. This last parameter is calculated as the plastic part of the chord rotation normalized to the yielding chord rotation θ_y. The adopted shear strength formula is reported in Equation (3).

$$V_R = \frac{1}{\gamma_{el}}\left[\frac{h-x}{2L_V} min(N; 0.55A_c f_c) + \left(1 - 0.05\, min\left(5; \mu_\Delta^{pl}\right)\right) \cdot \left[0.16\, max(0.5; 100\rho_{tot})\left(1 - 0.16\, min\left(5; \frac{L_V}{h}\right)\right)\sqrt{f_c}A_c + V_W\right]\right] \quad (3)$$

where: γ_{el} is equal to 1.15 for primary seismic elements, h is the depth of the cross-section, x is the compression zone depth, L_V is the ratio moment/shear at the end section, N is the compressive axial force, A_c is the cross-section area, f_c is the concrete strength, μ_Δ^{pl} is the plastic part of the chord rotation normalized to the yielding chord rotation, ρ_{tot} is the total longitudinal reinforcement ratio, V_W is the contribution of transverse reinforcement to shear resistance.

In this formula, mean values of the material properties divided by the partial factors are considered to calculate the shear resistance, in accordance with Eurocode criteria for safety verifications of brittle failure modes. Moreover, the resistance is updated at each step of the analysis depending on the actual ductility demand. In addition, if the ductility demand is lower than 1, the value of shear resistance is calculated with the expression defined for members not requiring shear reinforcement, given in Eurocode 2, part 1-1 [46].

3.3 CWSTs dissipative devices

The CWST dissipative devices are introduced in frame B (see Figure 3), i.e. the retrofitted one. The devices are modelled in Midas GEN through the use of two *link* elements working in parallel:

- a non-linear symmetric element with property type *SLIP bilinear* (link 1 element in Figure 3b) which simulates the cyclic behavior of the devices before the attainment of

the maximum deformation capacity. A yielding strength F_{eq} equal to 30 kN and an initial stiffness is 30'000 kN/m are considered. This element works symmetrically in order to represent the presence of two CWSTs equipped at each beam-column node;

- a non-linear symmetric element with *SLIP bilinear* property defined with an initial gap of 7.5 cm (link 2 element in Figure 3b), which simulates the behavior of the devices after the attainment of the maximum deformation S_{max} capacity. It is modelled with a symmetric behavior in order to consider the maximum displacement of both tubes. The yielding strength and the stiffness of this element are set with significantly high values, so that to model a rigid hinged connection between beams and columns.

A couple of link elements with the aforementioned properties is modelled at the top of each column, connecting beams to columns, to represent a set of seismic devices working in the horizontal direction of the ground-motion. At the top of the internal column, an additional horizontal rigid link is modelled in order to connect the seismic devices to both beam ends, as shown in Figure 3. It is worth saying that a vertical support is guaranteed for each node of the beams through appropriate settings in the software.

Friction was not implemented in the models because of the uncertainty in the determination of the parameters that control this mechanism, i.e. the definition of the coefficient of friction, the combination of horizontal and vertical components of the seismic action, and the energy dissipation related to friction. Considering a frictional mechanism in the model would imply to admit the benefits of friction energy dissipation that cannot be considered to be constant, and on which it is not always possible to rely because of the variations of the axial load in columns, due to the vertical component of the ground-motion. Furthermore, standard provisions do not allow to consider friction in the seismic response of structures.

Nevertheless, the contribution of friction in terms of maximum force transferred to columns, has been take into account in the selection of the yielding strength capacity of the dissipative devices adopted in this case study. Indeed, the value of the equivalent force of plasticization F_{eq} (see Section 2) for the CWSTs, was selected to be lower than the maximum value of force that could be transferred to the top of the columns without yielding their base sections.

Consequently, the column exhibits a certain degree of overstrength in order to guarantee that the sum of friction threshold force and of forces transmitted by the CWST devices, is lower than the force that would lead to the formation of a plastic hinge at the base. This is in accordance with the design criterion of this retrofit intervention, aimed at having columns performing linear elastic until the devices reach their maximum deformation capacity. Therefore, F_{eq} plus the contribution of frictional forces, has to be lower that the force activating yielding in columns, i.e. about 43 kN in for the external columns, and 54 kN for the central column, for the frame under analysis.

4 TIME-HISTORY ANALYSES

The first step of this Section consists in performing linear modal analysis to estimate the first period of vibration of the existing frame. For this purpose, model A is implemented in a linear model without the three plastic hinges at the base of the columns, but considering the cracked stiffness of the columns, following Eurocode 8 prescriptions [38]. In particular, a reduction coefficient for the moment of inertia of each column has been evaluated, so that to consider the secant lateral stiffness at yielding of each column. The result of this analysis is a first period of vibration T_1 of 1.561 seconds, for which almost the entire modal mass of the structure is participating. Indeed, precast RC structures are typically simple and strongly dominated by one vibrating mode [31].

4.1 Selection of the records

The seismic input adopted for the non-linear dynamic analyses is a set of 7 spectrum-compatible ground acceleration time histories. The target spectrum for the selection is the life safety limit state elastic response spectrum, defined by the Italian building code [47] for the site of Carpi (MO) in Italy. This spectrum has a return period of 712 years, corresponding, to a nominal life equal to 50 years and importance class III. Ground type C with no topographic amplification effects is assumed. The 7 accelerograms used in the analyses were selected from the NGA-West database developed by PEER [48], with the following *ad hoc* algorithm: i) only earthquakes with moment magnitude between 4 and 6 and recording stations with source-to-site shorter than 30 km are considered; ii) pulse-like ground-motions are excluded; iii) recordings not usable for periods up to 3.0 s are excluded [49]; iv) all spectra of the remaining accelerograms are scaled to the PGA of the target spectrum; v) response spectra with scaling factors higher than 3.0 or lower than 0.4 are excluded; vi) the scaled spectra are sorted based on ascending values of the average root-mean-square deviation of the observed spectrum from the target (DRMS) [49] in a range of periods from 1.0 s to 3.0 s; vii) all the possible combinations of 7 spectra are considered among the 10 scaled spectra with the lowest DRMS values; viii) for each combination of 7 spectra the DRMS value for the mean spectrum is computed; ix) the 7 spectra with the mean spectrum with the lowest DRMS value are identified.

The selected scaled spectra are plotted in Figure 4, and the corresponding ground-motion data are reported in Table 2. In particular, the earthquake name and year are indicated, together with the name of the recording station, the Joyner-Boore source-to-site distance R_{JB}, the moment magnitude (M_w), the direction of the horizontal component with reference to the NGA classification [48], the peak ground acceleration PGA, and the scaling factor SF^0.

Following Eurocode 8 recommendations [38] when seven ground motions are used, the average result of the response quantities from the analyses is adopted to compute the value of the action effect.

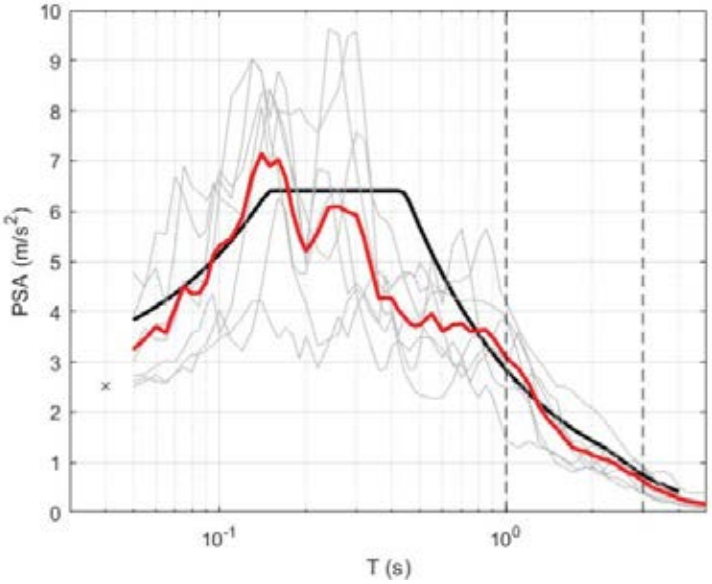

Figure 4: Scaled response rectum for each of the 7 accelerograms selected (gray lines), average spectrum (red), and target code spectrum for spectral compatibility in the range of periods spanning from 1.0 s to 3.0 s. The PGA is indicated with the symbol ×. All the accelerograms are scaled to the same PGA.

N°	Earthquake name, Year [-]	Station name [-]	R_{JB} distance [km]	M_w [-]	Component [-]	PGA [m/s^2]	SF^0 [-]
TH1	Chalfant Valley-01, 1986	Bishop - LADWP South St	23.38	5.77	H1	1.270	1.982
TH2	Chalfant Valley-01, 1986	Bishop - LADWP South St	23.38	5.77	H2	0.926	2.717
TH3	Westmorland, 1981	Brawley Airport	15.28	5.90	H1	1.660	1.516
TH4	Westmorland, 1981	Salton Sea Wildlife Refuge	7.57	5.90	H2	1.729	1.455
TH5	Coyote Lake, 1979	Gilroy Array #3	6.75	5.74	H2	2.242	1.122
TH6	San Salvador, 1986	National Geografical Inst	3.71	5.80	H1	3.987	0.631
TH7	Coyote Lake, 1979	Gilroy Array #3	6.75	5.74	H1	2.673	0.941

Table 2: Main parameters of the seven accelerograms selected.

4.2 Non-linear analyses

Non-linear time history analyses have been performed on both model A (frame with hinged connections) and model B (frame retrofitted with CWSTs), with the purpose of estimating, for each accelerogram, the scaling factor that leads to the attainment of one of the ultimate conditions of the structure. In particular, each record is gradually scaled until one of these collapse conditions is reached: (i) ultimate chord rotation in one of the three columns; (ii) cyclic shear resistance in one of the three columns. It is worth saying that the scaling of the time-histories is performed with factors SF^1 on the records already scaled with the SF^0 introduced for the spectra compatibility. The scaling factors SF^1 are reported up to the first decimal digit. Therefore, the i-th accelerogram is actually scaled by $SF_i = SF_i^0 \cdot SF_i^1$.

The non-linear analyses are carried out with Rayleigh damping, calculated based on the first and the second periods of vibration (see Section 4.1), considering 5% damping ratio. P-Delta effects are also taken into account in the analyses, even if not particularly significant for this frame, since the columns are characterized by low axial loads.

For each analysis, the time histories of the following response parameters are evaluated: the shear in columns, the displacements at the top of columns, the chord rotations of columns, the hysteretic behavior of the CWSTs and of the plastic hinges. As mentioned before, the analyses are conducted considering three different values of the ultimate chord rotations:

- Rotation Limit RL1 - Ultimate chord rotations calculated with Equation (2);
- Rotation Limit RL2 - 80% of the values of the ultimate chord rotations adopted in RL1;
- Rotation Limit RL3 - 60% of the values of the ultimate chord rotations adopted in RL1.

As an example, some significant results are proposed for models A and B, referring to the accelerogram TH6, for a scaling factor SF^1 equal to 1, for the ultimate chord rotations capacity RL1. Figure 5 shows moment-rotation plots for the left and the central column of the frame, for the model A (black line) and the model B (red line). In the model A, the rotation in all plastic hinges exceeds the yielding point, while in the model B, all columns remain elastic. Moreover, in model B, one of the CWST devices in each couple at the top of the three columns, reaches the maximum deformation capacity S_{max}. Therefore, the three link 2 elements (see Section 3.3) are activated, transferring the full effect of seismic actions from beams to columns. This effect is visible in Figure 6, which shows the non-linear force-deformation cyclic behaviors of the three devices in model B. The cyclic behavior link 1 elements are shown in Figure 6a, these have a deformation capacity S_{max} equal to 7.5 cm, then the link 2 elements are activated (Figure 6b).

With the subsequent increase of the scaling factor SF^1 of time history TH6, the yielding of the plastic hinges of columns gradually occurs also in model B. However, the three columns in

model A reach the ultimate rotation values for a SF^1 equal to 1.30, lower than the one corresponding to model B, which is equal to 1.70. Furthermore, for all time histories, it can be observed that the plastic hinges of the columns in model B remain elastic until the CWST devices attain their ultimate deformation capacity. This confirms that the CWSTs in model B, allow to guarantee a higher performance against the ultimate rotation capacity of columns.

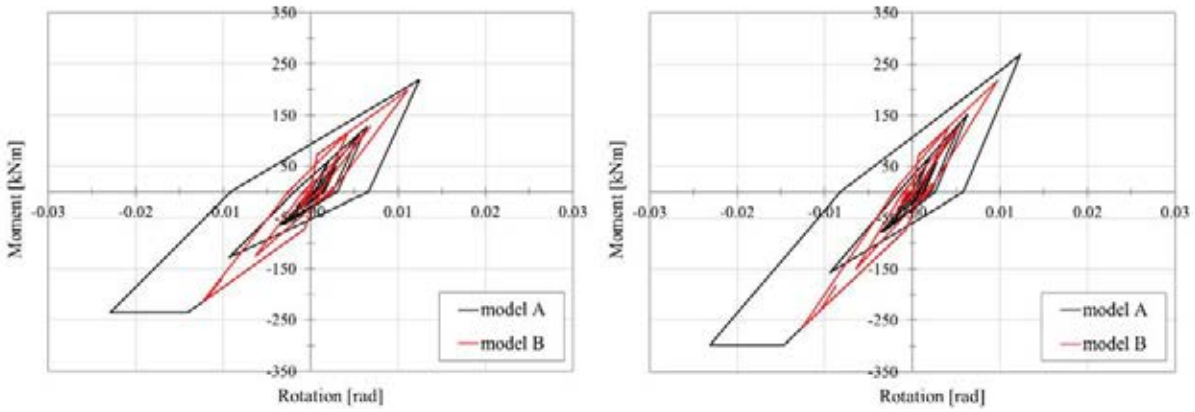

Figure 5: Cyclic behavior of columns plastic hinges for model A (black line) and model B (red line), for time history TH6 and $SF^1 = 1$: a) left column the frame; b) central column of the frame.

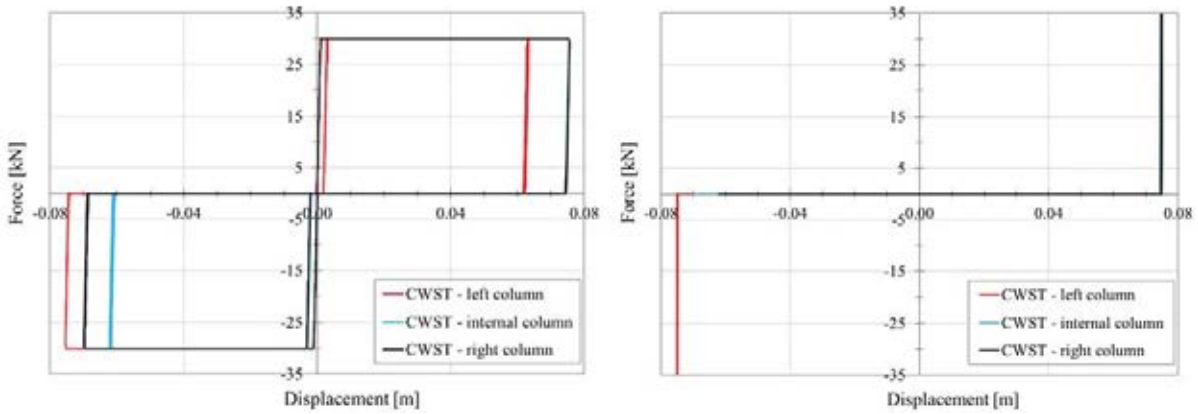

Figure 6: Cyclic behavior of the three CWSTs at the beam-column nodes in model B, for time history TH6 and $SF^1 = 1$: a) cyclic behavior of link 1 (see Section 3.3); b) cyclic behavior of link 2 (see Section 3.3).

In order to further evaluate the influence of the CWSTs, the time-histories of the deformations in the plastic hinge, and the shear in the left column of the frame, are proposed in Figure 7 and 8, for the accelerogram TH2 and the rotation limit RL1. Figure 7a and 8a refer to a scaling factor $SF^1 = 1.5$ for both models, while Figure 7b and 8b refer to a scaling factor $SF^1 = 2$. In Figure 7, the positive effect of the devices can be observed in terms of lower deformations in model B compared to model A. Figure 8a shows that the left column in model A reaches a value of shear that corresponds to the yielding of the plastic hinge (about 43 kN), while the left column in model B has lower shear values. Indeed, for a scaling factor $SF^1 = 1.5$, all the columns in model A are yielded, while all the columns in model B are still elastic.

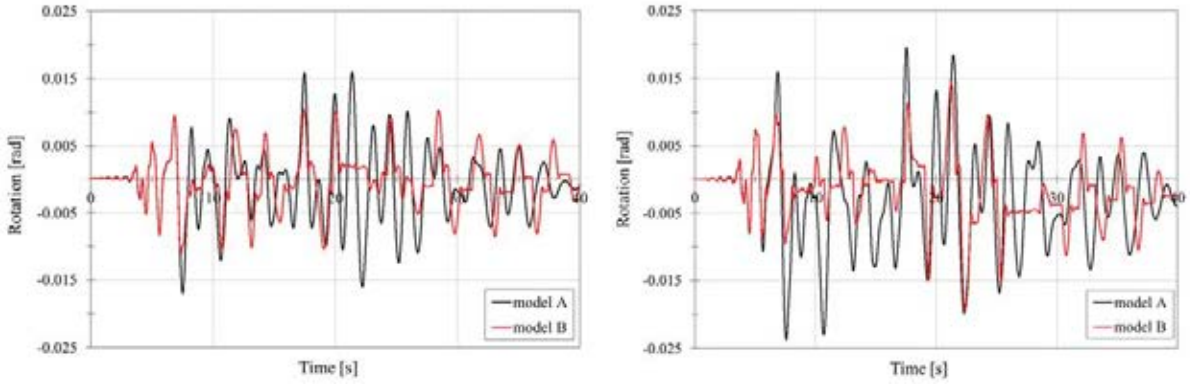

(a) (b)

Figure 7: Time-histories of the chord rotation of the left column for TH2, for model A (black line) and model B (red line): a) $SF^1 = 1.5$; b) $SF^1 = 2.0$.

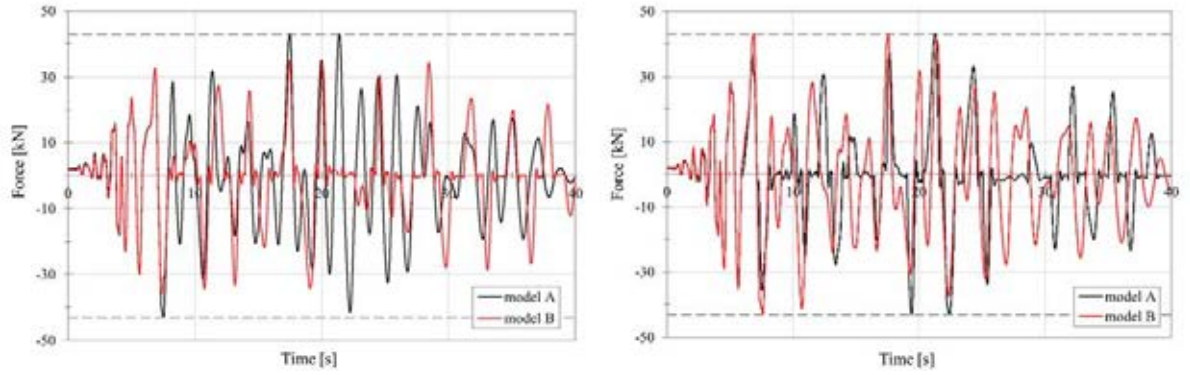

(a) (b)

Figure 8: Time-histories of the base shear for the left column for TH2, for model A (black line) and model B (red line): a) $SF^1 = 1.5$; b) $SF^1 = 2.0$.

For $SF^1 = 2$, Figure 8b, it is possible to observe that the left column reaches the yielding force both in model A and B. However, in Figure 7b it can be noticed that, even if the left column is yielded in both models, the deformation of the plastic hinge in model B is lower than in model A. This is the positive effect of the activation of the CWSTs in the non-linear model B.

As mentioned before, the different values of chord rotations influence also the calculation of the resistance against cyclic shear. For the left column of the frame with $SF^1 = 2$, that is equal to 82.3 kN for model A and 135.7 kN for model B. Whereas, for $SF^1 = 2$, they decrease to 80.6 kN and 81.7 kN, respectively. Indeed, due to the fact that the ductility demand is higher in model A, the shear resistance is lower than the one found for model B, for both scaling factors. In any case, the shear strength of columns is always higher than the shear value corresponding to the maximum flexural capacity of the plastic hinges, therefore no shear failure is predicted by the analyses. Therefore, the base shear at the ultimate condition is equal for systems with and without CWSTs, so the verifications depend on the value of chord rotations only.

Table 3 summarizes the scaling factors to be used in models A and B in order to achieve the ultimate rotation of the plastic hinges at the base of columns, considering the three different rotation limits RL defined at the beginning of the present section. The positive effect of the CWSTs is generally visible, since the model B reaches the collapse condition for higher scaling factors compared to model A. However, ground-motion record TH1 has an opposite behavior for the rotation limit RL1. Anyway, this effect is not observed considering all the other cases.

This particular behavior can be attributed to the insurgence of dynamic amplifying effects in model B for this specific record, at scaling factors SF^1 higher than 2.8. Indeed, for lower scaling factors, the positive action of the CWSTs is again evident in model B. As expected, the lowest scaling factors for both models A and B among the three thresholds considered, are found for RL3, corresponding to 60% reduction of the ultimate chord rotations.

N°	SF^0	RL1: θ_u		RL2: 80% θ_u		RL3: 60% θ_u	
		SF^1 model A	SF^1 model B	SF^1 model A	SF^1 model B	SF^1 model A	SF^1 model B
TH1	1.982	3.20	2.90	2.70	2.80	2.00	2.30
TH2	2.717	2.80	3.20	2.40	2.80	1.60	2.00
TH3	1.516	3.10	3.90	2.70	3.50	2.10	2.30
TH4	1.455	3.80	5.20	3.40	4.40	2.20	3.00
TH5	1.122	1.80	3.10	1.50	2.30	1.10	1.80
TH6	0.631	1.30	1.70	1.10	1.50	0.90	1.30
TH7	0.941	3.60	6.20	3.00	5.10	2.40	3.60

Table 3: Scaling factors SF^1 for each of the seven accelerograms adopted in the time-history analyses, for model A and model B, corresponding to the three chord rotation limits considered.

5 BEHAVIOR FACTOR ESTIMATION

The evaluation of the behavior factor for the existing structure (Model A), and for the structure equipped with CWSTs (Model B), is discussed out is this section. The behavior factor q is calculated as:

$$q = \frac{V_{b,el}}{V_{b,nl}} \tag{4}$$

where $V_{b,nl}$ is the maximum base shear calculated from the non-linear analyses described in Section 4.2, with a ground-motion scaling factor bringing each model to the ultimate chord rotation, and $V_{b,el}$ is the maximum base shear in an equivalent elastic structure with the same base acceleration. For all the limits of ultimate chord rotation considered, $V_{b,nl}$ is constant and equal to 140 kN while the corresponding scaling factor for each accelerogram is reported in Table 3, with reference to the three different rotation limits RL. The absolute values of $V_{b,el}$ obtained from the equivalent elastic model are reported Table 4. This model is similar to model A, but it does not have plastic hinges at the base of columns.

N°	$V_{b,nl}$ [kN]	RL1: θ_u		RL2: 80% θ_u		RL3: 60% θ_u	
		$V_{b,el}$ [kN] model A	$V_{b,el}$ [kN] model B	$V_{b,el}$ [kN] model A	$V_{b,el}$ [kN] model B	$V_{b,el}$ [kN] model A	$V_{b,el}$ [kN] model B
TH1	140	483	441	412	427	309	354
TH2	140	493	558	427	493	289	359
TH3	140	375	466	328	421	257	281
TH4	140	440	591	395	506	258	350
TH5	140	318	528	267	401	197	318
TH6	140	371	471	318	422	263	371
TH7	140	341	543	289	460	234	341

Table 4: Absolute values of the base shear calculated in the time-history analyses of the linear frame model. See Table 3 for the corresponding scaling factors for the accelerograms.

As an example, the time histories of the base shear for the equivalent linear model are reported in Figure 9, for TH7. In particular, Figure 9a concerns RL1 and shows with a black line the base shear $V_{b,el}$, calculated with a scaling factor $SF^1 = 3.6$ obtained from model A, and with a red line $V_{b,el}$ calculated with $SF^1 = 6.2$, obtained from model B. The value of $V_{b,nl}$ is also reported with a dashed line. Clearly, since the model is fully linear, the time histories are simply scaled. Figure 9b illustrates the same results for RL3, corresponding to the 60% reduction of the ultimate chord rotation thresholds. The plots correspond to $SF^1 = 2.4$ for frame A, and $SF^1 = 3.6$ for frame B. In this case, with a lower threshold for the ultimate condition compared to the previously discussed case, the gap between the results of frames A and B is lower. This is probably due to the aforementioned amplifying dynamic effects observed at higher values of the scaling factors.

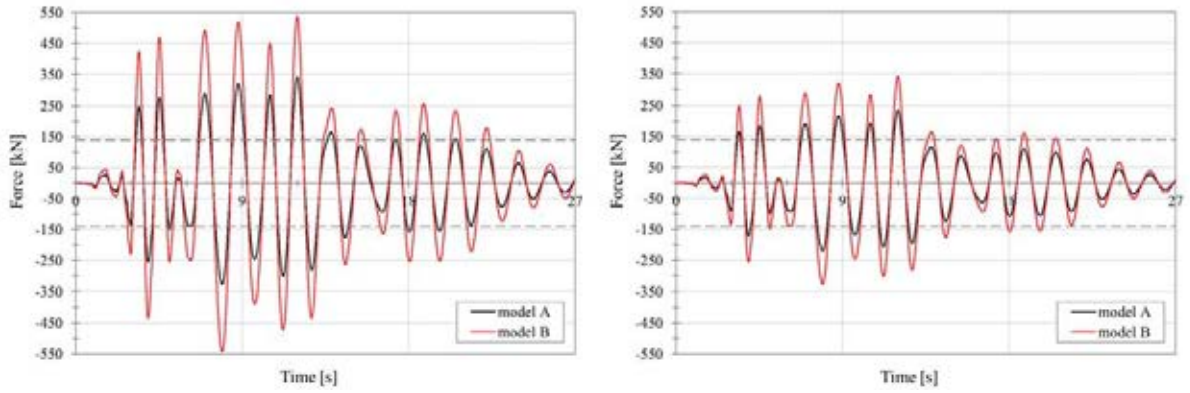

Figure 9: Time-histories of the base shear $V_{b,el}$ for record TH7, for model A (black line) and model B (red line): a) results for RL1 with threshold θ_u; b) results for RL3 with threshold 60% θ_u.

Table 5 reports the behavior factor values calculated with Equation (4) for each RL, and the corresponding average values in the bottom row. The same values are plotted in Figure 10, showing the variability of q for the seven accelerograms adopted, for each model. On average, the variability of q is consistent with the values observed for the precast buildings analyzed in Pollini et al. [32].

It is worth noticing that the same behavior factors are obtained for TH5, TH6 and TH7, both for model A for RL1, and for model B for RL3. These results for the two models are not correlated, and they are probably due to the fact the scaling factors SF^1 are calculated up to the first decimal digit. If additional analyses were performed, considering more refined scaling factors, the results would likely differ for the two models.

As expected, the adoption of different ultimate chord rotations in columns affect significantly the results, since in RL2 and RL3 there is a consistent reduction in the behavior factors with respect to RL1. In particular for what concerns the model A, the average behavior factors for RL2 and 3 are 14% and 36% lower than the value obtained for RL1, respectively. Similarly for the model B, the behavior factors are 13% and 34% smaller compared to RL1 results.

Eurocode 8 part 1 [38], would recommend to adopt a behavior factor lower than 1.5 for a newly designed precast structure without seismic detailing. Moreover, Eurocode 8 part 3 [39] suggests to adopt a behavior factor not higher than 1.5 for an existing reinforced concrete structure for which the available ductility is not specifically justified. Since the columns of the existing frame under analysis are characterized by poor transversal reinforcement and are not designed against seismic actions, the average behavior factor of 2.88 obtained for model A is

deemed to have a certain degree of overestimation. The result is considered to be more realistic for this case study, when a reduction of the ultimate chord rotation is introduced. In particular, q decreases from 2.88, to 2.49 with a collapse limit 80% of θ_u, and to 1.84 with a collapse limit 60% of θ_u. These results clearly depend on the ultimate rotation limits predicted by Equation (2), which are not specific for existing precast columns, therefore, additional research is necessary in order to find more suitable formulations to be applied to this structural typologies, as recognized also by Magliulo et al. [45].

N°	RL1: θ_u		RL2: 80% θ_u		RL3: 60% θ_u	
	q model A	q model B	q model A	q model B	q model A	q model B
TH1	3.45	3.15	2.94	3.05	2.21	2.53
TH2	3.52	3.98	3.05	3.52	2.06	2.56
TH3	2.68	3.33	2.34	3.01	1.83	2.00
TH4	3.14	4.22	2.82	3.61	1.84	2.50
TH5	2.27	3.77	1.90	2.87	1.41	2.27
TH6	2.65	3.36	2.27	3.01	1.88	2.65
TH7	2.44	3.88	2.06	3.29	1.67	2.44
Average values	**2.88**	**3.67**	**2.49**	**3.19**	**1.84**	**2.42**

Table 5: Behavior factors estimated for model A and model B, for the seven records adopted in the time-history analyses, for the three ultimate Rotation Limits considered.

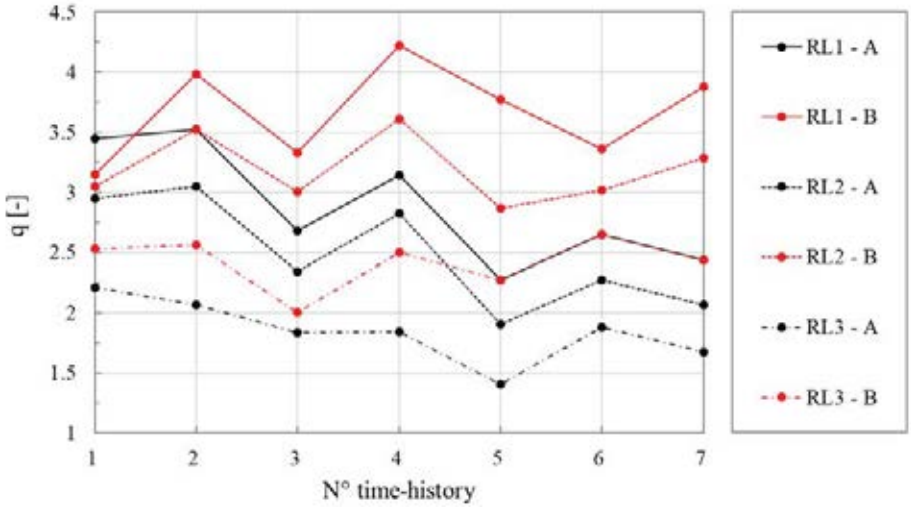

Figure 10: Behavior factor calculated for model A and B, for the three RL scenarios considered.

6 CONCLUSIONS

The paper discusses the seismic retrofit of an existing precast RC building equipped with CWSTs at beam-column joints. Non-linear time-history analyses have been conducted on two different models of the main frame of the structure, one with hinged beam-column connections representing the existing condition (model A), and on the one with CWST devices (model B). The effects of the introduction of the CWSTs in the connections is evaluated in terms of chord rotations demand on the columns and base shear forces, and equivalent behavior factors are proposed for the two structures. The sensitivity of the outcomes depending on the ultimate

chord rotations of columns is analyzed considering three rotation limits. On the basis of the results of the numerical simulations, the following conclusions can be drawn:

- In general, the maximum chord rotations of columns observed in the frame model with CWSTs are lower than the maximum values observed in the frame model with hinged connections, at the same scaling factor of the records, i.e. under the same seismic action;
- The damage mechanism of columns is in fully agreement with the design criteria adopted for the intervention, since, in all the analyses, the columns in model B do not yield until the attainment of the maximum deformation of the devices;
- Equivalent behavior factors are calculated for model A and model B, for three threshold values of ultimate chord rotations;
- The behavior factors estimated for model B are always higher than the ones estimated for model A, featuring simple hinged connections: the increase of the mean values of behavior factor is about 30% for model B with dissipative devices;
- The behavior factor depends on the ultimate chord rotation of columns considered, showing that the behavior factor significantly decreases with the decrease of θ_u;
- Additional analyses adopting other formulations for the calculation of θ_u are required in order to find realistic results for the specific case of evaluating existing precast columns; moreover, further research may be necessary for the modelling of the non-linear flexural behavior of precast elements;
- CWST devices are deemed to be a good solution for maintaining a low level of stress and deformation in the existing columns of the frame, since frame model B is less vulnerable than frame model A, under the same seismic actions.

AKNOWLEDGEMENTS

The support of Sismocell - Sismo Solution s.r.l., is gratefully acknowledged.

REFERENCES

[1] A. Belleri, E. Brunesi, R. Nascimbene, M. Pagani, P. Riva, Seismic performance of precast industrial facilities following major earthquakes in the italian territory. *Journal of Performance of Constructed Facilities*, **29**(5): 04014135, 2014. https://doi.org/10.1061/(ASCE)CF.1943-5509.0000617

[2] M. Savoia, N. Buratti, L. Vincenzi, Damage and collapses in industrial precast buildings after the 2012 Emilia earthquake. *Engineering Structures*, **137**, 162-180, 2017. https://doi.org/10.1016/j.engst ruct.2017.01.059

[3] N. Buratti, F. Minghini, E. Ongaretto, M. Savoia, N. Tullini, Empirical seismic fragility for the precast RC industrial buildings damaged by the 2012 Emilia (Italy) earthquakes. *Earthquake Engineering & Structural Dynamics*, **46**, 2317-2335, 2017. https://doi.org/10.1002/eqe.2906

[4] F. Minghini, E. Ongaretto, V. Ligabue, M. Savoia, N. Tullini, Observational failure analysis of precast buildings after the 2012 Emilia earthquakes. *Earthquake Structures*, **11**(2), 327-346, 2016. https://doi.org/10.12989/eas.2016.11.2.327

[5] N. Batalha, H. Rodrigues, H. Varum, Seismic performance of RC precast industrial buildings—learning with the past earthquakes. *Innovative Infrastructure Solutions*, **4**(4), 2019. https://doi.org/10.1007/s41062-018-0191-y

[6] D.A. Bournas, P. Negro, F.F. Taucer, Performance of industrial buildings during the Emilia earthquakes in Northern Italy and recommendations for their strengthening. *Bulletin of Earthquake Engineering*, **12**, 2383-2404, 2013. https://doi.org/10.1007/s10518 - 013 - 9466 - z

[7] L. Liberatore, L. Sorrentino, D. Liberatore, L.D. Decanini, Failure of industrial structures induced by the Emilia (Italy) 2012 earthquakes. *Engineering Failure Analysis*, **34**, 629-647, 2013. https://doi.org/10.1016/j.engfailanal.2013.02.009

[8] G. Magliulo, M. Ercolino, C. Petrone, O. Coppola, G. Manfredi, The Emilia earthquake: seismic performance of precast reinforced concrete buildings. *Earthquake Spectra*, **30**, 891-912, 2014. https://doi.org/10.1193/091012EQS285M

[9] A. Babič, M. Dolšek, Seismic fragility functions of industrial precast building classes. *Engineering Structures*, **118**, 357-370, 2016. https://doi.org/10.1016/j.engstruct.2016.03.069

[10] C. Demartino, I. Vanzi, G. Monti, C. Sulpizio, Precast industrial buildings in Southern Europe: loss of support at frictional beam-to-column connections under seismic actions. *Bulletin of Earthquake Engineering*, **16**, 259-294, 2018. https://doi.org/10.1007/s1051 8-017-0196-5

[11] M. Bovo, M. Savoia, Evaluation of force fluctuations induced by vertical seismic component on reinforced concrete precast structures. *Engineering Structures*, **179**, 70-87, 2019. https://doi.org/10.1016/j.engstruct.2018.10.018

[12] A. Titi, F. Biondini, G. Toniolo, Seismic assessment of existing precast structures with dry-friction beam-to-column joints. *Bulletin of Earthquake Engineering*, **16**, 2067-2086, 2018. https://doi.org/10.1007/s10518-017-0271-y

[13] F. Biondini, A. Titi, G. Toniolo. Biondini F, Titi A, Toniolo G, Prestazioni sismiche di strutture prefabbricate con connessioni trave - pilastro ad attrito (in Italian). *Proceedings of the XV Conference of the Italian Association of Seismic Engineering (ANIDIS)*, Padua, Italy, 30 June-4 July, 2013.

[14] M. Ercolino, G. Magliulo, G. Manfredi, Failure of a precast RC building due to Emilia-Romagna earthquakes. *Engineering Structures*, **118**, 262-273, 2016. http://dx.doi.org/10.1016/j.engstruct.2016.03.054

[15] M. Bovo, M. Savoia, Numerical simulation of seismic-induced failure of a precast structure during the Emilia earthquake. *Journal of Performance of Constructed Facilities*, **32**(1): 04017119, 2018. https://doi.org/10.1061/(ASCE)CF.1943-5509.0001086

[16] M.G. Deyanova, S. Pampanin, R. Nascimbene, Assessment of single-storey precast concrete industrial buildings with hinged beam-column connections with and without dowels. *Second European conference on earthquake engineering and seismology*, Istanbul, Turkey, 25-29 August, 2014.

[17] V. Ligabue, M. Bovo, M. Savoia, Connessioni tegolo-trave: studio sperimentale e numerico del comportamento di angolari di collegamento (in Italian). *Proceedings of workshop "Tecniche innovative per il miglioramento sismico di edifici prefabbricati"*, Bologna, Italy, 22 October, 2014.

[18] G. Muciaccia, M. Cervio, M. Franzoso, M. Veneziano, Utilizzo di ancoraggi post-inseriti in interventi di recupero di capannoni industriali in zona sismica (in Italian). *Proceedings of Workshop "Tecniche innovative per il miglioramento sismico di edifici prefabbricati"*, Bologna, Italy, 22 October, 2014.

[19] E. Nastri, M. Vergato, M. Latour, Performance evaluation of a seismic retrofitted R.C. precast industrial building. *Earthquake and Structures*, **12**(1), 13-21, 2017. https://doi.org/10.12989/eas.2017.12.1.013

[20] L. Rossi, M. Stupazzini, D. Parisi, B. Holtschoppen, G. Ruggieri, C. Butenweg, Empirical fragility functions and loss curves for Italian business facilities based on the 2012 Emilia-Romagna earthquake official database. *Bulletin of Earthquake Engineering*, **18**, 1693-1721, 2020. https://doi.org/10.1007/s10518-019-00759-1

[21] D. Rodrigues, H. Crowley, V. Silva, Earthquake loss assessment of precast RC industrial structures in Tuscany (Italy). *Bulletin of Earthquake Engineering*, **16**, 203-228, 2017. https://doi.org/10.1007/s10518-017-0195-6

[22] M. Bosio, A. Belleri, P. Riva, A. Marini, Displacement-based simplified seismic loss assessment of Italian precast buildings. *Journal of Earthquake Engineering*, **24**(1), 60-81, 2020. https://doi.org /10.1080/13632469.2020.1724215

[23] B. Dal Lago, F. Biondini, G. Toniolo, Friction-based dissipative devices for precast concrete panels. *Engineering Structures*, **147**, 356-371, 2017. https://doi.org/10.1016/J.ENGST RUCT.2017.05.050

[24] B. Dal Lago, F. Biondini, G. Toniolo, Experimental investigation on steel W-shaped folded plate dissipative connectors for horizontal precast concrete cladding panels. *Journal of Earthquake Engineering*, **22**(5), 778-800, 2017. https://doi.org/10.1080/13632469.2016.1264333

[25] B. Dal Lago, G. Toniolo, R. Felicetti, M. Lamperti Tornaghi, End support connection of precast roof elements by bolted steel angles. *Structural Concrete*, **18**(5), 755-767, 2017. https://doi.org/10.1002/suco.201600218

[26] R. Scotta, L. De Stefani, R. Vitaliani, Passive control of precast building response using cladding panels as dissipative shear walls. *Bulletin of Earthquake Engineering*, **13**, 3527-3552, 2015. https://doi.org/10.1007/s10518-015-9763-9

[27] A. Belleri, A. Marini, P. Riva, R. Nascimbene, Dissipating and re-centring devices for portal-frame precast structures. *Engineering Structures*, **150**, 736-745, 2017. https://doi.org/10.1016/j.engstruct.2017.07.072

[28] P. Martinelli, M.G. Mulas, An innovative passive control technique for industrial precast frames. *Engineering Structures*, **32**, 1123-1132, 2010. https://doi.org/10.1016/j.engstruct.2009.12.038

[29] L. Marinini, P. Spatti, P. Riva, R. Nascimbene, Strutture prefabbricate: moderni sistemi di protezione antisismica (in Italian). *Progettazione sismica*, **3**, 23-44, 2011.

[30] A.V. Pollini, N. Buratti, C. Mazzotti, Effectiveness of a dissipative beam-column connection based on carbon-wrapped steel tubes. *Second European conference on earthquake engineering and seismology*, Istanbul, Turkey, 25-29 August, 2014.

[31] A.V. Pollini, N. Buratti, C. Mazzotti, Experimental and numerical behaviour of dissipative devices based on carbon-wrapped steel tubes for the retrofitting of existing precast RC structures. *Earthquake Engineering & Structural Dynamics*, 1-21, 2018. https://doi.org/10.1002/eqe.3017

[32] A.V. Pollini, N. Buratti, C. Mazzotti, Behavior factor of concrete portal frames with dissipative devices based on carbon-wrapped steel tubes. *Bulletin of Earthquake Engineering*, **19**, 553-578, 2021. https://doi.org/10.1007/s10518-020-00977-y

[33] H-W. Song, Z-M. Wan, Z-M. Xie, X-W. Du, Axial impact behavior and energy absorption efficiency of composite wrapped metal tubes. *International Journal of Impact Engineering*, **24**(4), 385-401, 2000. https://doi.org/10.1016/S0734-743X(99)00165-7

[34] R.M. Lima, Z.N. Ismarrubie, E.S. Zainudin, S.H. Tang, Axial behavior of steel tube wrapped by composite as energy absorber under compressive load, *IEEE Symposium on Business, Engineering and Industrial Applications* (ISBEIA), Langkawi, Malaysia, 2011.

[35] M. Savoia, C. Mazzotti, N. Buratti, B. Ferracuti, M. Bovo, V. Ligabue, L. Vincenzi, Damages and collapses in industrial precast buildings after the Emilia earthquake (in Italian). *Ingegneria Sismica*, **29**(2), 120-131, 2012.

[36] D. Bellotti, C. Casotto, H. Crowley, M.G. Deyanova, F. Germagnoli, G. Fianchisti, E. Lucarelli, S. Riva, R. Nascimbene, Single-storey precast buildings: probabilistic distribution of structural systems and subsystems from the sixties (in Italian). *Progettazione Sismica*, **5**(3), 41-70, 2014.

[37] https://www.cspfea.net/prodotti/midas-gen/. Accessed 21 March 2021.

[38] CEN (European Committee for Standardization), Design of structures for earthquake resistance – Part 1: General rules, seismic actions and rules for building. *Eurocode 8*, Brussels, 2005.

[39] CEN (European Committee for Standardization), Design of structures for earthquake resistance – Part 3: Assessment and retrofitting of buildings. *Eurocode 8*, Brussels, 2005.

[40] T. Takeda, M.A. Sozen, N.N. Nielsen, Reinforced concrete response to simulated earthquake. *Journal of the structural division*, **96**(12), 2557-2573, 1970.

[41] D.E Biskinis, M.N. Fardis, Cyclic strength and deformation capacity of RC members, including members retrofitted for earthquake resistance. *Proceedings of the 5th International Ph.D Symposium in Civil Engineering*, Delft, Balkema, 1125-1133, 2004.

[42] D.E. Biskinis, M.N. Fardis, Cyclic deformation capacity, resistance and effective stiffness of RC members with or without retrofitting. *Proceedings of the 14th World conference on Earthquake Engineering*, Beijing, China, 12-17 October, 2008.

[43] G.M. Verderame, P. Ricci, G. Manfredi, E. Cosenza, Ultimate chord rotation of RC columns with smooth bars: some considerations about EC8 prescriptions. *Bulletin of Earthquake Engineering*, **8**, 1351-1373, 2010. https://doi.org/10.1007/s10518-010-9190-x

[44] M. Bovo, N. Buratti, Evaluation of the variability contribution due to epistemic uncertainty on constitutive models in the definition of fragility curves of RC frames. *Engineering Structures*, **188**, 700-716, 2019. https://doi.org/10.1016/j.engstruct.2019.03.064

[45] G. Magliulo, D. Bellotti, C. Di Salvatore, F. Cavalieri, RINTC-E project: towards the seismic risk of low and pre-code single-story RC precast buildings in Italy. *Proceedings of the 7th ECCOMAS Thematic Conference on Computational Methods in Structural Dynamics and Earthquake Engineering (COMPDYN)*, Crete, Greece, 24-26 June, 2019.

[46] CEN (European Committee for Standardization), Design of concrete structures – Part 1-1: General rules and rules for buildings. *Eurocode 2*, Brussels, 2004.

[47] D.M. 20/02/2018, Norme tecniche per le costruzioni (in Italian). Decreto ministeriale del Ministero delle Infrastrutture e dei trasporti, 2018.

[48] https://peer.berkeley.edu/nga-west. Accessed 21 March 2021.

[49] J.J. Boomer, A.B. Acevedo, The use of real earthquake accelerograms as input to dynamic analysis. *Journal of Earthquake Engineering*, **8**(1), 43-91, 2004.